# Elastic-stiffness coefficients of a silicon-carbide fiber at elevated temperatures: Acoustic spectroscopy and micromechanics modeling

By H. OGI[*], S. KAI[*], T. ICHITSUBO[*], M. HIRAO[*], and K. TAKASHIMA[**]

[*]*Graduate School of Engineering Science, Osaka University*
*Toyonaka, Osaka 560-8531, Japan*

[**]*Precision and Intelligence Laboratory, Tokyo Institute of Technology,*
*Yokohama, Kanagawa 226-8503, Japan*

KEYWORDS

Elastic Constants, Electromagnetic Acoustic Resonance, Metal-Matrix Composite, Micromechanics Modeling, Silicon-Carbide Fiber

ABSTRACT

We have determined all five independent elastic-stiffness coefficients $C_{ij}$ of a silicon-carbide fiber with transverse isotropy from room temperature up to 873 K. First, we measured the $C_{ij}$ of a Ti-alloy-matrix composite reinforced unidirectionally with the fibers and the matrix alloy alone. Electromagnetic acoustic resonance detected the free-vibration resonance frequencies of the specimens to determine their $C_{ij}$. Second, we applied a micromechanics calculation to deduce the fiber $C_{ij}$ from the measured composite and matrix $C_{ij}$. The resulting fiber $C_{ij}$ show strong anisotropy in the temperature derivatives of the $C_{ij}$; the temperature derivatives for the fiber-axis-direction $C_{ij}$ are much smaller than the others.

Contacting author: Hirotsugu Ogi (ogi@me.es.osaka-u.ac.jp)

Tel. +81-6-6850-6187, Fax. +81-6-6850-6188

## §1. INTRODUCTION

Silicon-carbide (SiC) fibers offer high strength, rigidity, and corrosion resistance at elevated temperatures. Reinforcing metals with them provides toughness as well, known as metal-matrix composites (MMC), and have found important applications in space/aeronautical structural elements (Johnson 1988; Wadworth and Froes 1998). A stand-alone single fiber would be useable for micromachines.

Designing such an application often requires the fiber's elastic-stiffness coefficients $C_{ij}$. Overall elastic constants of an MMC can be predicted from the fiber and matrix $C_{ij}$, for example. However, conventional methods are inapplicable to measuring all of the fiber $C_{ij}$ because of two principal reasons: (i) small fiber diameter (~0.14 mm) and (ii) strong elastic anisotropy showing many independent $C_{ij}$ (typically five). Conventional methods, such as the pulse-echo method, need many measurements on many oriented specimens in many directions for the anisotropic $C_{ij}$. This is an unrealistic task for fibers. The $C_{ij}$ measurements at elevated temperatures would pose further difficulties. Previous studies (Mittnick 1987; Jansson *et al*. 1991; Mital *et al*. 1994) have then measured only Young's modulus along the fiber-longitudinal direction for room temperature.

In this study, we determined all five $C_{ij}$ of the SiC fiber with transverse isotropy from room temperature up to 873 K. The procedure takes two steps: (i) measurements of the $C_{ij}$ of an MMC, which is composed of an isotropic Ti-alloy matrix and the fibers embedded unidirectionally, and the $C_{ij}$ of the matrix alloy alone; and (ii) a micromechanics calculation for deducing the fiber $C_{ij}$ from the composite $C_{ij}$, the matrix $C_{ij}$, and the fiber volume fraction. The composite and matrix $C_{ij}$ are measured with electromagnetic acoustic resonance (EMAR) (Ogi, Ledbetter, Kim, and Hirao, 1999; Ogi, Takashima et al. 1999; Ogi et al. 2000); free-vibration resonance frequencies of a well-shaped specimen depend on the dimensions, mass density, and all the material's $C_{ij}$. Measurement of the resonance frequencies then permits us to inversely

determine the $C_{ij}$ with the known dimensions and mass density. The EMAR technique makes a contactless acoustic coupling possible and allows choosing an individual vibration group from eight possible groups of a rectangular parallelepiped specimen. This aspect prevents mode misidentification and guarantees high accuracy of the deduced elastic constants. The subsequent micromechanics calculation uses Mori-Tanaka (1973) mean-field theory. We cite a study by Ledbetter, Datta, and Kyono (1989) who have inversely determined the elastic constants of graphite fibers using conventional ultrasonic measurements and a plane-wave theory.

## §2. MATERIAL

We consider a continuous SCS-6 SiC fiber. It consists of a carbon core surrounded by SiC as shown in fig. 1. The fiber diameter is 140 μm. Such an annular structure macroscopically exhibits transverse isotropy with five independent $C_{ij}$:

$$\left[C_{ij}\right]=\begin{bmatrix} C_{11} & C_{12} & C_{13} & 0 & 0 & 0 \\ & C_{11} & C_{13} & 0 & 0 & 0 \\ & & C_{33} & 0 & 0 & 0 \\ & & & C_{44} & 0 & 0 \\ & & & & C_{44} & 0 \\ & & & & & C_{66} \end{bmatrix}. \qquad (1)$$

Hence $C_{66}=(C_{11}-C_{12})/2$.

The composite material is a Ti-6Al-4V alloy unidirectionally reinforced with the SiC fibers. The fiber volume fraction is 0.35. The material was fabricated by a foil-fiber-foil technique (8 plies) at 1173 K uncer a 65-MPa hydrostatic pressure. We take the $x_3$ axis along the fiber-longitudinal direction and the $x_2$ axis normal to the foil plane throughout this study. We prepared a rectangular-parallelepiped specimen, measuring about 4.5 mm by 1.7 mm by 4.0 mm along the $x_1$, $x_2$, and $x_3$ axes, respectively. Figure 2 shows the microstructure seen along the $x_3$

direction. The Archimedes-method mass density was 3.879 g/cm$^3$. We also prepared a rectangular-parallelepiped specimen of the matrix alloy alone for measuring its isotropic $C_{ij}$.

## §3. MEASUREMENT

Figure 3 shows our EMAR apparatus for measuring the free-vibration resonance frequencies of the composite and matrix-alloy specimens. The specimen was inserted in a solenoid coil located within a stainless-steel cylindrical container. A heater surrounding the coil raises the temperature at a rate of 0.8 K/min. The pressure the container was kept less than $10^{-4}$ Torr. (Deterioration occurred at the SiC-carbon interfaces due to oxidization over 700 K when the specimen was exposed to air (Ogi *et al*. 2001).) A pair of permanent magnets was located outside the container to apply the static magnetic field to the specimen for the electromagnetic excitation and detection of free vibration. The field direction is changeable by rotating the permanent magnets about the container axis to select the detecting vibration modes.

We applied high-power tone bursts to the solenoid coil to vibrate the specimen via the Lorentz forces. The specimen was under *free* vibration because the coil was loose and never tight; the applied force to the specimen was only its own weight. After the excitation, the same coil received the vibration through the reversed-Lorentz-force mechanism. The received signals entered superheterodyne phase detectors and the amplitude spectrum at the operating frequency was obtained. Frequency scans provided many resonance peaks. The resonance frequencies were determined by the Lorentzian-function fitting. An inverse calculation for the measured and calculated resonance frequencies (Ohno 1976; Migliori and Sarrao 1997; Ledbetter et al. 1995) derived all the independent elastic-stiffness coefficients of the specimen. Mode identification for the measured resonance frequencies, which is the key in the inverse calculation, was correctly made through choosing the vibration modes. This mode-selection principle is described in detail by Ogi, Ledbetter, Kim, and Hirao (1999).

## §4. MICROMECHANICS CALCULATION

We consider the $SiC_f$/Ti-alloy composite to be a dual-phase composite consisting of the matrix with isotropic symmetry and the aligned fibers with transverse isotropic symmetry. The effective elastic-stiffness coefficients of the composite $\mathbf{C}^c$ can be expressed with the strain concentration factor of the fiber, **A**, as (Dunn and Ledbetter, 1995)

$$\mathbf{C}^c = \mathbf{C}^m + v_f\left(\mathbf{C}^f - \mathbf{C}^m\right)\mathbf{A}. \tag{2}$$

Here, $\mathbf{C}^m$ and $\mathbf{C}^f$ denote the elastic-stiffness matrices of the matrix and fiber, respectively. $v_f$ is the fiber volume fraction. We estimate **A** using the mean-field theory by Mori and Tanaka (1973) as:

$$\begin{cases} \mathbf{A} = \mathbf{A}_D\left[(1-v_f)\mathbf{I} + v_f\mathbf{A}_D\right]^{-1} \\ \mathbf{A}_D = \left[\mathbf{I} + \mathbf{S}\left\{\mathbf{C}^m\right\}^{-1}\left(\mathbf{C}^f - \mathbf{C}^m\right)\right]^{-1} \end{cases}. \tag{3}$$

Here **I** denotes the identity matrix. **S** denotes the Eshelby tensor and is a function of the fiber shape and $\mathbf{C}^m$. When the matrix is isotropic, the expressions of the **S** components are simple for the fiber shape (the long circular cylinder) and they are tabulated in Mura's monograph (1987). When the matrix is anisotropic, the **S** components can be numerically calculated as shown by Kinoshita and Mura (1971). The simplified expression for the cylinder-cylindrical inclusions is

$$S_{ikmn} = \frac{1}{4\pi}\int_c \frac{C^m_{jlmn}\xi_l\left(\xi_k N_{ij} + \xi_i N_{kj}\right)}{D}dr. \tag{4}$$

Here, $\xi_l$ denotes a component of the unit vector lying normal to the fiber axis, and $N_{ij}$ and D denote the cofactor matrix and determinant of matrix $G_{ij} = C^m_{ipjq}\xi_p\xi_q$, respectively. The integration is made along the unit circle surrounding the fiber at the center. Equation (4) has been verified by Ichitsubo *et al.* (2002).

Equations (2) and (3) give

$$\mathbf{C}^{\mathrm{f}} = \left[ \left(\mathbf{C}^{\mathrm{c}} - \mathbf{C}^{\mathrm{m}}\right)\mathbf{S}\left\{\mathbf{C}^{\mathrm{m}}\right\}^{-1} - \frac{\mathrm{v_f}}{\mathrm{v_m}}\mathbf{I} \right]^{-1} \left[ \left(\mathbf{C}^{\mathrm{c}} - \mathbf{C}^{\mathrm{m}}\right)\mathbf{S} + \mathbf{C}^{\mathrm{m}} - \frac{1}{\mathrm{v_m}}\mathbf{C}^{\mathrm{c}} \right], \tag{4}$$

where $v_m$=1-$v_f$, the matrix volume fraction. Thus, measurements of $\mathbf{C}^c$, $\mathbf{C}^m$, and $v_f$ permit us to determine the fiber elastic stiffnesses $\mathbf{C}^f$.

## §5. RESULT

Figure 4 shows the resonance spectra of the composite specimen at various temperatures: Capability of mode selection and good signal-to-noise ratio demonstrate the EMAR's usefulness for the $C_{ij}$ measurement at elevated temperatures. Shifts to lower frequencies indicate the elastic softening with temperature increase. Figure 5 shows temperature dependence of the composite $C_{ij}$, which shows linear decreases with temperature without hysteresis. The matrix $C_{ij}$ also showed linear decreases up to 900 K. (Note that the α–β phase transition occurs near 1000 K in the matrix.) The rms difference between the measured and calculated resonance frequencies after the inverse calculations was typically 0.8% for the composite material. This indicates that the transverse-isotropy assumption for the composite is allowable with this error. The rms difference for the isotropic matirix was 0.2%. Figure 6 shows the temperature dependence of the fiber $C_{ij}$. The scattered results for $C_{33}$, $C_{11}$ and the bulk modulus $B$ are attributable to their weak contributions to the resonance frequencies. Table I gives the normalized temperature derivatives of the composite $C_{ij}$, the matrix $C_{ij}$, and the fiber $C_{ij}$. Table II gives the fiber $C_{ij}$ at room temperature together with those of the composite and matrix.

## §6. DISCUSSION

First, we discuss the reliability of the resulting fiber $C_{ij}$. A direct comparison with a previous study is impracticable because no study has reported a complete set of the fiber $C_{ij}$. But, there are reports on the tensile-test Young's modulus $E_3$ along the fiber longitudinal

direction at room temperature. The values reported range from 400 to 428 GPa (Mittnick 1987; Jansson *et al*. 1991; Mital *et al*. 1994), which our fiber $E_3$ falls within.

Further confirmation is made possible by measuring and calculating the $C_{ij}$ of such a composite that contains another alignment of the fibers. We prepared a crossply composite for this purpose; the Ti-alloy matrix reinforced by the fibers along the two principal directions alternately (0°/90° crossply) (Ogi, Takashima *et al*. 1999). The fiber volume fraction was 0.35. This composite macroscopically shows tetragonal symmetry with six independent $C_{ij}$. We measured them with the EMAR method. On the other hand, the micromechanics modeling calculations allow calculation of the crossply-composite $C_{ij}$ with the known matrix $C_{ij}$, the fiber volume fraction, and the determined fiber $C_{ij}$. The calculated and measured coefficients are compared with each other in Table III. We see good agreement between them, especially for the diagonal $C_{ij}$. This favorable comparison supports our fiber $C_{ij}$.

We have assumed that the polycrystalline Ti-alloy matrix of the composite is elastically isotropic. However, it might not be the case because the composite was fabricated by the foil-fiber-foil technique; a texture may occur. Thus, the matrix can exhibit transverse isotropy with five independent $C_{ij}$. We investigated the effect of matrix anisotropies on the resultant fiber $C_{ij}$, simulating various transverse anisotropy of the matrix with the same bulk modulus. (The bulk modulus is independent of texture.) We varied the shear-modulus anisotropy ( $\mathbf{C}_{66}^{\mathrm{m}} - \mathbf{C}_{44}^{\mathrm{m}}$ anisotropy) and the longitudinal-modulus anisotropy ( $\mathbf{C}_{33}^{\mathrm{m}} - \mathbf{C}_{11}^{\mathrm{m}}$ anisotropy). The results are shown in fig. 7. A 30% $\mathbf{C}_{66}^{\mathrm{m}} - \mathbf{C}_{44}^{\mathrm{m}}$ anisotropy causes errors less than 3% in the fiber $C_{ij}$. This anisotropy corresponds to the shear-modulus anisotropy of monocrystal titanium, indicating that the fiber $C_{ij}$ are insensitive to $\mathbf{C}_{66}^{\mathrm{m}} - \mathbf{C}_{44}^{\mathrm{m}}$ anisotropy. A 10% $\mathbf{C}_{33}^{\mathrm{m}} - \mathbf{C}_{11}^{\mathrm{m}}$anisotropy, corresponding to the longitudinal-modulus anisotropy of monocrystal titanium, causes errors less than 3%, except for the fiber $C_{11}$. (The fiber $C_{11}$ is sensitive to the $\mathbf{C}_{33}^{\mathrm{m}} - \mathbf{C}_{11}^{\mathrm{m}}$ anisotropy.) The texture would cause elastic anisotropy in the matrix, but the relative magnitude would be

less than a few percent, confirming our view that the deduced fiber $C_{ij}$ are little affected by the matrix anisotropy. This result is related to the fiber $C_{ij}$ much larger than the matrix $C_{ij}$. Thus, our assumption of isotropy for the matrix yields a reliable set of the fiber $C_{ij}$.

Next, we discuss the temperature derivatives of the fiber $C_{ij}$. We observe a large difference between the fiber's longitudinal and radial directions; the derivative for $C_{33}$ is smaller in magnitude than that for $C_{11}$ by a factor 4.7 and that for $E_3$ smaller than for $E_1$ by a factor 3.0. This is perhaps attributed to (i) nearly temperature-independent elastic constants of the carbon core and/or (ii) anisotropic elastic constants of the SiC and carbon. The fiber itself is a composite consisting of the SiC and carbon core. A micromechanics calculation for an isotropic SiC with an isotropic carbon core reveals that the carbon's elastic constants most affect the $C_{33}$ and $E_3$ of the composite fiber. Thus, the temperature derivatives of the fiber $C_{33}$ and $E_3$ highly depend on those of the carbon's elastic constants. If the SiC and carbon are elastically anisotropic, anisotropy in the temperature derivative will occur.

## §7. CONCLUSIONS

The present study gives the complete set of elastic-stiffness coefficients $C_{ij}$ of the silicon-carbide fiber from room temperature to 873 K. The results were confirmed in two ways via Young's modulus along the fiber axis and anisotropic elastic-stiffness coefficients of the crossply composite. The micromechanics calculation for an anisotropic matrix revealed that the deduced fiber $C_{ij}$ were little affected by the matrix anisotropy. The temperature derivatives of the $C_{ij}$ along the fiber axis are much smaller than those for the others. Those results will be useful for predicting the anisotropic elastic constants of composites containing the SiC fibers. The technique presented here is applicable to any other continuos fibers, including those with much smaller diameters.

**REFERENCES**

Dunn, M. and Ledbetter, H., 1995, *J. Appl. Mech.*, **62**, 1023.

Ichitsubo, T., Tane, M., Ogi, H., Hirao, M., Ikeda, T., and Nakajima, H., 2002, *Acta Materialia*, in press.

Jansson, S., Deve, H., and Evans, A., 1991, *Met. Trans. A*., **22A**, 2975.

Johnson, W., Lubowinski, S., Highsmith, A., Brewer, W., and Hoogstraten, C., 1988, *NASA Technical Report*, NASP TM-1014.

Ledbetter, H., Datta, S., and Kyono, T., 1989, *J. Appl. Phys.*, **65**, 3411.

Ledbetter, H., Fortunko, C., and Heyliger, P., 1995, *J. Appl. Phys.*, **78**, 1542.

Kinoshita, N., and Mura, T., 1971, *Phys. Stat. Solid.*, **A5**, 759.

Migliori, A. and Sarrao, J., 1997, *Resonant Ultrasound Spectroscopy*, Wiley, New York.

Mital, S., Chamis, C., and Gotsis, P., 1994, Comp. Sci. Tech., **50**, 59.

Mittnick, M., 1987, in *Metal Matrix Composite*, Dvorak, G. and Zweben, C. eds., Technomic Publishing, Lancaster, PA.

Mochizuki, E., 1987, *J. Phys. Earth*, **35**, 159.

Mori, T. and Tanaka, K., 1973, *Acta Metall.*, **21**, 571.

Mura, T., 1987, in *Micromechanics of Defects in Solids*, 2nd edn., Martinus Nijhoff, The Hague.

Ogi, H., Ledbetter, H., Kim, S., and Hirao, M., 1999, *J. Acoust. Soc. Am.*, **106**, 660.

Ogi, H., Takashima, K., Ledbetter, H., Dunn, M., Shimoike, G., Hirao, M., and Bowen, P., 1999, *Acta Mater*., **47**, 2787.

Ogi, H., Dunn, M. L., Takashima, K., Ledbetter, H., 2000, *J. Appl. Phys.*, **87**, 2769.

Ogi, H., Ledbetter, H., Takashima, K., Shimoike, G. and Hirao, M., 2001, *Met. Mater. Trans.* A., **32A**, 425.

Ohno, I., 1976, *J. Phys. Earth*, **24**, 355.

Wadsworth, J. and Froes, F., 1989, *J. Met.*, **41**, 12.

Table Caption

TABLE I Temperature derivatives of the elastic constants $(dC/dT)/C$ ($10^{-4}$ $K^{-1}$) of the unidirectional $SiC_f$/Ti-6Al-4V composite, Ti-6Al-4V alloy, and SiC fiber.

TABLE II Elastic constants (GPa) of the unidirectional $SiC_f$/Ti-6Al-4V composite, Ti-6Al-4V alloy, and SiC fiber at 293 K. The fiber longitudinal direction is along the $x_3$ axis.

TABLE III Measured and calculated constants (GPa) of the crossply $SiC_f$/Ti-6Al-4V with tetragonal symmetry at 293 K. Two principal axes of the fiber are along the $x_1$ and $x_2$ axes, respectively.

TABLE I

| | $C_{11}$ | $C_{33}$ | $C_{44}$ | $C_{66}$ | $E_1$ | $E_3$ | B |
|---|---|---|---|---|---|---|---|
| composite(SiC/Ti-6Al-4V) | -2.5 | -1.3 | -4.5 | -4.2 | -3.6 | -1.9 | -1.3 |
| matrix(Ti-6Al-4V) | -2.8 | -2.8 | -4.7 | -4.7 | -4.4 | -4.4 | -1.8 |
| SiC fiber | -1.4 | -0.3 | -3.9 | -2.1 | -1.8 | -0.6 | -0.4 |

TABLE II

| | $C_{11}$ | $C_{33}$ | $C_{12}$ | $C_{13}$ | $C_{44}$ | $C_{66}^{*}$ | $E_1$ | $E_3$ | B |
|---|---|---|---|---|---|---|---|---|---|
| composite (SiC/Ti-6Al-4V) | 195 | 253 | 85.4 | 72.2 | 53.9 | 54.8 | 150 | 216 | 121 |
| matrix (Ti-6Al-4V) | 161 | 161 | 76.2 | 76.2 | 42.7 | 42.4 | 113 | 113 | 105 |
| SiC fiber | 299 | 425 | 106 | 62 | 86.3 | 96.5 | 258 | 406 | 163 |

* $C_{66}=(C_{11}-C_{12})/2$

TABLE III

| | $C_{11}$ | $C_{33}$ | $C_{44}$ | $C_{66}$ | $C_{12}$ | $C_{13}$ |
|---|---|---|---|---|---|---|
| measurement | 226 | 189 | 54.7 | 52.1 | 81.9 | 78.4 |
| calculation | 225 | 192 | 55.2 | 55.1 | 72 | 73.9 |
| diff.(%) | 0.4 | -1.6 | -0.9 | -5.8 | 12.1 | 5.7 |

Figure Caption

Fig. 1 Microstructure of the silicon carbide fiber (SCS-6). The fiber consists of a carbon core and silicon carbide surrounding the core. The bar indicates 20 μm.

Fig. 2 Microstructure of the $SiC_f$/Ti-6Al-4V composite. The bar indicates 200 μm.

Fig.3 EMAR-measurement setup at elevated temperatures.

Fig.4 Resonance spectra of the $SiC_f$/Ti composite material at various temperatures. (a) $B_{1g}$ vibration modes and (b) $A_g$ vibration modes. Mode notation follows Mochizuki (1987).

Fig. 5 Temperature dependence of the elastic constants of the unidirectional $SiC_f$/Ti-6Al-4V composite. Solid marks denote measurements in the heating process and open ones in the cooling process.

Fig. 6 Temperature dependence of the elastic constants of the SiC fiber. Solid marks denote measurements in the heating process and open ones in the cooling process.

Fig. 7 Sensitivities the fiber elastic constants to the hexagonal matrix anisotropy; (a) effect of the shear-modulus anisotropy and (b) effect of the longitudinal-modulus anisotropy. The bulk modulus of the matrix is the same as that of the isotropic case.

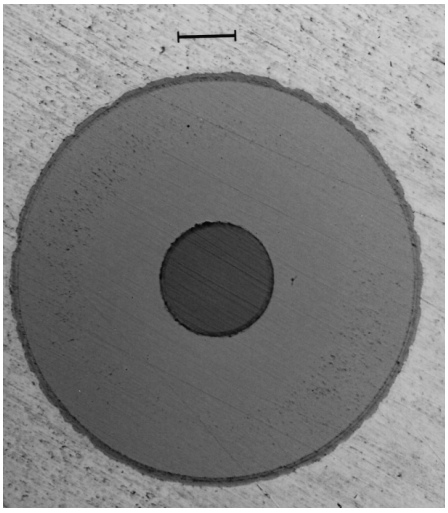

Fig. 1

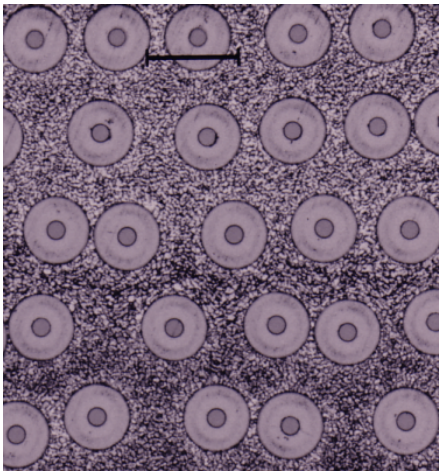

Fig. 2

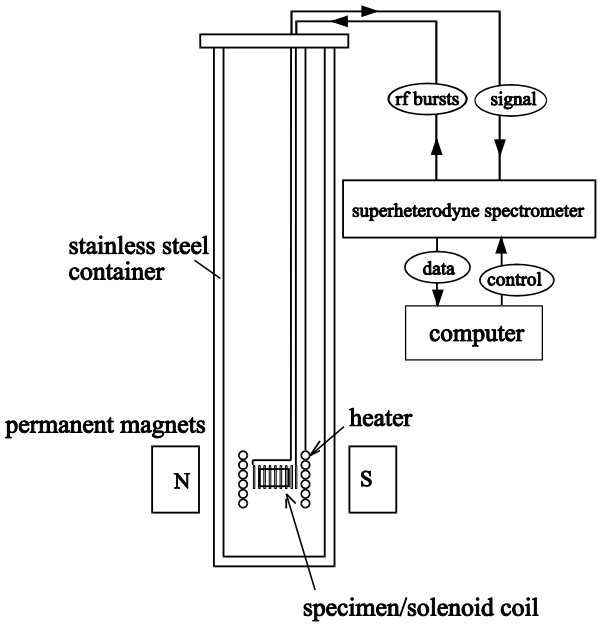
rf bursts
signal
superheterodyne spectrometer
data
control
computer
stainless steel
container
permanent magnets
heater
N
S
specimen/solenoid coil

Fig.3

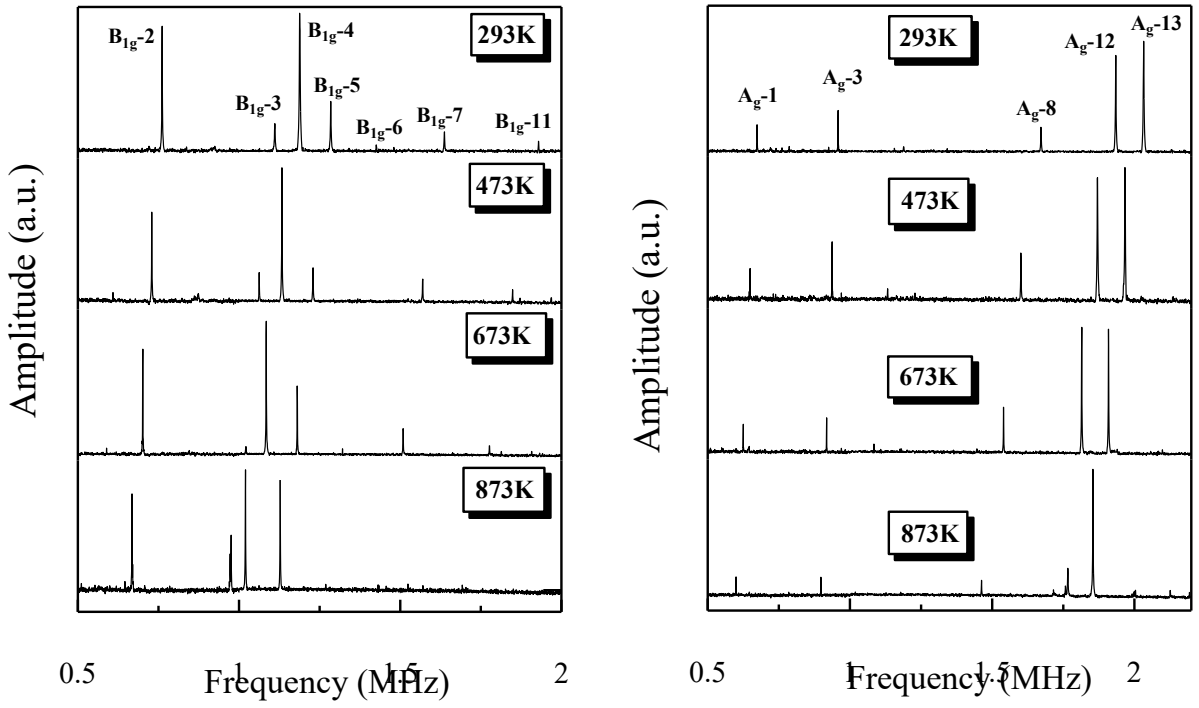
Amplitude (a.u.)
B1g-2
B1g-3
B1g-4
B1g-5
B1g-6
B1g-7
B1g-11
293K
473K
673K
873K
0.5
1
1.5
2
Frequency (MHz)
(a)
Amplitude (a.u.)
Ag-1
Ag-3
Ag-8
Ag-12
Ag-13
293K
473K
673K
873K
0.5
1
1.5
2
Frequency (MHz)
(b)

Fig.4

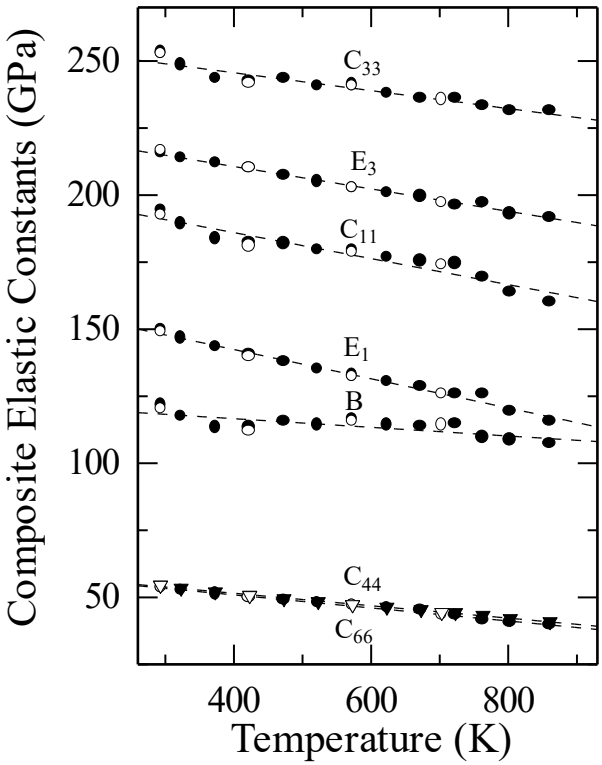
Composite Elastic Constants (GPa)
250
200
150
100
50
400
600
800
Temperature (K)
C33
E3
C11
E1
B
C44
C66

Fig. 5

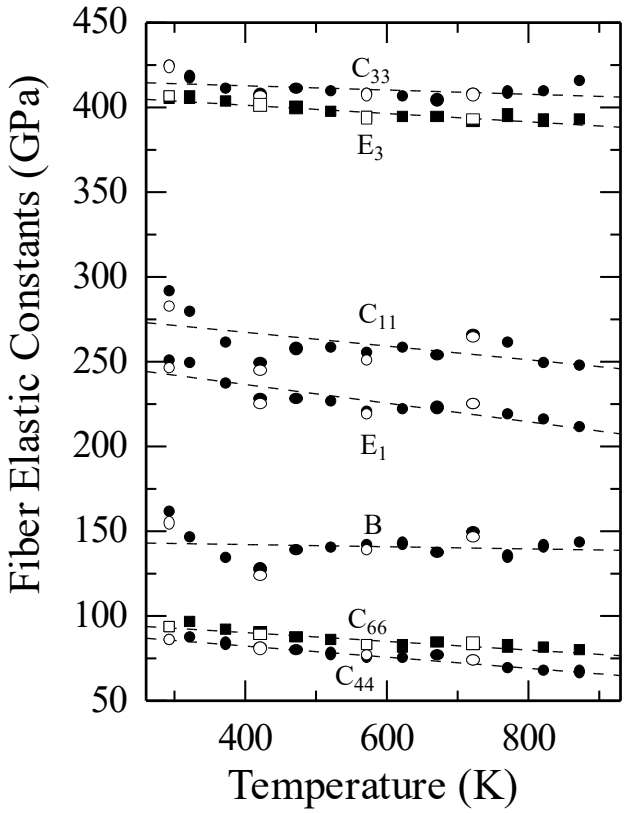
Fiber Elastic Constants (GPa)
Temperature (K)
450
400
350
300
250
200
150
100
50
400
600
800
C33
E3
C11
E1
B
C66
C44

Fig. 6

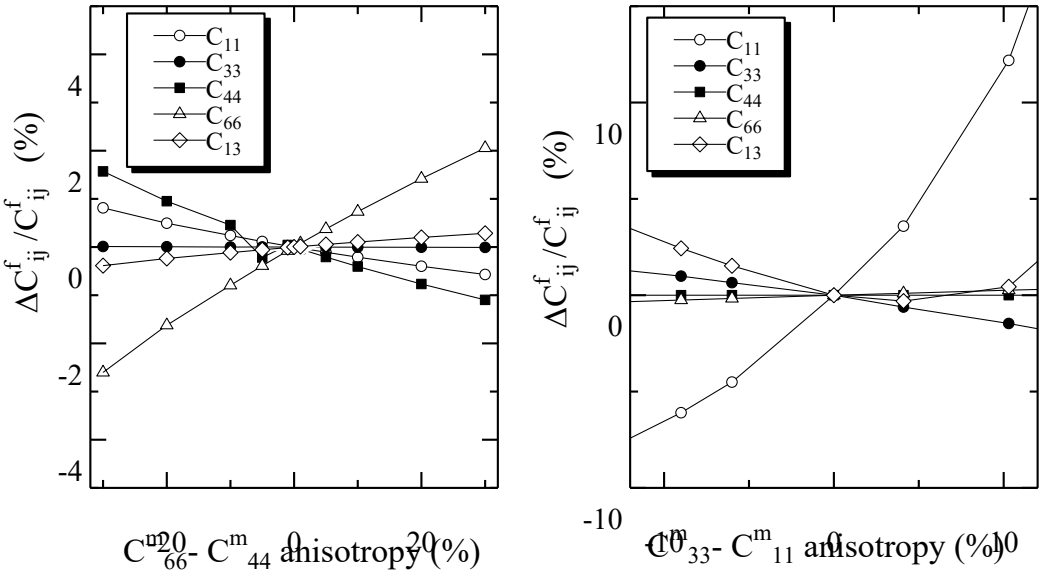
$C_{11}$
$C_{33}$
$C_{44}$
$C_{66}$
$C_{13}$
$\Delta C^f_{ij}/C^f_{ij}$ (%)
4
2
0
-2
-4
-20
0
20
$C^m_{66}$- $C^m_{44}$ anisotropy (%)
10
0
-10
-10
0
10
$C^m_{33}$- $C^m_{11}$ anisotropy (%)

Fig. 7